RESEARCH LETTER

Key Points:
- An enhanced AMOC leads to a southward shift and steepened isopycnals in the GS
- Nutrient reservoirs in the GS region move along with the steepened isopycnals
- Biogeochemical variability in the GS region is linked to the GS path and AMOC

Impact of the Atlantic meridional overturning circulation on the decadal variability of the Gulf Stream path and regional chlorophyll and nutrient concentrations

A. Sanchez-Franks[1] and R. Zhang[2]

[1]National Oceanography Centre, Southampton, UK, [2]Geophysical Fluid Dynamics Laboratory, NOAA, Princeton, New Jersey, USA

Abstract In this study, we show that the underlying physical driver for the decadal variability in the Gulf Stream (GS) path and the regional biogeochemical cycling is linked to the low frequency variability in the Atlantic meridional overturning circulation (AMOC). There is a significant anticorrelation between AMOC variations and the meridional shifts of the GS path at decadal time scale in both observations and two Earth system models (ESMs). The chlorophyll and nutrient concentrations in the GS region are found significantly correlated with the AMOC fingerprint and anticorrelated with the GS path at decadal time scale through coherent isopycnal changes in the GS front in the ESMs. Our results illustrate how changes in the large-scale ocean circulation, such as AMOC, are teleconnected with regional decadal physical and biogeochemical variations near the North American east coast. Such linkages are useful for predicting future physical and biogeochemical variations in this region.

1. Introduction

The Gulf Stream (GS) transports warm salty water from the subtropical region to midlatitudes, affecting the entire troposphere [*Minobe et al.*, 2008]. Changes in the GS path can induce changes in winter synoptic atmospheric variability [*Joyce et al.*, 2009] and have a strong impact on changes in the marine ecosystem/fisheries, such as the spatial distribution of silver hake over the last 40 years [*Nye et al.*, 2011].

The interannual migration of the GS path has been linked to the winter North Atlantic Oscillation (NAO) [*De Coetlogon et al.*, 2006; *Frankignoul et al.*, 2001; *Joyce et al.*, 2000; *Taylor and Stephens*, 1998], the deep western boundary current (DWBC) [*Thompson and Schmitz*, 1989], and the entrainment of the upper DWBC [*Spall*, 1996]. The NAO can affect the GS path through both wind-driven gyre circulation and buoyancy-driven overturning circulation [*Marshall et al.*, 2001; *Kwon et al.*, 2010]. The meridional shift of the GS path in the open ocean and the strength of the cyclonic northern recirculation gyre (NRG) north of the GS are found linked to the strength of the deep branch of the Atlantic meridional overturning circulation (AMOC) through interaction with bottom topography and the associated bottom vortex stretching, in both high and coarse resolution Geophysical Fluid Dynamics Laboratory (GFDL) models [*Zhang and Vallis*, 2007; *Zhang et al.*, 2011]. Similar results are also found in the National Center for Atmospheric Research ocean general circulation model [*Yeager and Jochum*, 2009]. These modeling results are supported by observations showing the latitude of the GS path significantly anticorrelated with the AMOC fingerprint [*Joyce and Zhang*, 2010].

Previous studies suggested that the nutrient supply around the GS is caused by the along-isopycnal nutrient advection in the GS [*Jenkins and Doney*, 2003; *Pelegri and Csanady*, 1991; *Schollaert et al.*, 2004] and originates from the nutrient-rich subsurface waters in the western Sargasso Sea [*Csanady*, 1990]. This is consistent with *Kremeur et al.* [2009], showing that the nutrient distribution and primary production were largely driven by the advection through gyre circulation. Other studies [*Williams et al.*, 2006; *Palter and Lozier*, 2008] suggest an alternative tropical source for the GS nutrients.

Satellite observations reveal an anticorrelation between sea surface temperature (SST) and ocean surface chlorophyll concentrations [*Behrenfeld et al.*, 2006; *Martinez et al.*, 2009]. In regions with abundant light, increased (decreased) vertical mixing can bring more (fewer) nutrients to the phytoplankton population and enhance (reduce) the phytoplankton bloom [*Doney*, 2006; *Follows and Dutkiewicz*, 2002]. In addition to

changes in SSTs, vertical mixing and phytoplankton biomass can also be strongly impacted by changes in wind and buoyancy forcing [*Lozier et al.*, 2011].

In this study, we revisit the linkage between the meridional migration of the GS path and the AMOC variability at decadal time scale, using both observed data and the control simulation from two Earth system models (ESMs). We also investigate the impact of AMOC variability on the marine biogeochemical cycle in the GS region using the two ESMs.

2. Data and Methods

The observed data are from the objectively analyzed data sets of ocean temperature anomalies from 1955 to 2014 [*Levitus et al.*, 2005], and the model outputs are from 500 year control simulations of two EMSs (GFDL ESM2M and ESM2G) [*Dunne et al.*, 2013, 2012]. The main differences between the two ESMs are the vertical coordinates in the ocean components; ESM2M employs *z* coordinates, while ESM2G uses isopycnal coordinates.

A classic measure for the GS path is the latitude of the 15°C isotherm at 200 m [*Cornillon and Watts*, 1987; *Fuglister and Voorhis*, 1965]. Here for both simulated and observed results, our estimates for the GS path are obtained from zonally averaged locations of the annual mean 15°C isotherm at 200 m between 75°W and 55°W, similar to that used in previous studies [*Joyce and Zhang*, 2010; *Joyce et al.*, 2009]. This observed GS index is detrended over the entire period (1955–2014). It correlates well with the GS index used in *Joyce and Zhang* [2010] (both are normalized, detrended, and 5 year smoothed for their overlapping period) (Figure S1 in the supporting information; $r = 0.82$, significant at 99% level). Because there were no continuous observations of AMOC before the RAPID program started in 2004 [*Cunningham et al.*, 2007], we use an AMOC fingerprint (the leading mode of the detrended annual mean ocean subsurface temperature at 400 m in the extratropical North Atlantic) for both observed and simulated results as suggested in previous studies [*Mahajan et al.*, 2011; *Zhang*, 2008]. A positive AMOC fingerprint corresponds to warming in the subpolar gyre and cooling in the GS region (Figures 1b and 1d in *Zhang* (2008)). The principal component of this leading mode (PC1) is highly correlated with the volume transport-based AMOC index [*Zhang*, 2008]. The PC1 explains 30%, 20%, and 25% of variance in observation, ESM2M, and ESM2G, respectively. For reference, we note that the volume transport-based AMOC index (here defined as the maximum of the zonally integrated Atlantic meridional overturning streamfunction in depth-space at 26°N) and the AMOC fingerprint, both with the 5 year running smooth, have a zero-lag correlation of 0.73 and 0.85 in ESM2M and ESM2G, respectively, statistically significant at 99% level.

The impact of AMOC variability on the marine biogeochemical cycle in the GS region is also investigated using the two ESMs. The index for the biogeochemical variables in the GS region are derived using EOF analysis over the subdomain, 80°W–50°W and 35°N–45°N. The chlorophyll index in the euphotic zone is defined as PC1 of the annual mean chlorophyll concentrations at 35 m depth over the subdomain. The chlorophyll response to changes in the GS path was found to be largest at 25 m in ESM2M and at 35 m in ESM2G, respectively. In ESM2M, the chlorophyll response at 35 m is slightly smaller but very similar to that at 25 m. Hence, 35 m was the chosen depth for chlorophyll index in both ESMs. Correspondingly, the nutrient index at the base of the euphotic zone is defined as the PC1 of the annual mean phosphate (PO_4) concentrations at 150 m depth over the subdomain. For both ESMs, the maximum anticorrelation between nutrient and GS path was found to be at 150 m; hence, 150 m was the chosen depth for the nutrient index.

To focus on the variability at decadal time scale, all indexes (both physical and biogeochemical variables) in this paper are smoothed with a 5 year running mean unless otherwise specified. The equivalent uncorrelated sample size (n') for the degrees of freedom (i.e., $df = n' - 2$) in a serial correlation is defined here as

$$n' = \frac{n}{1 + \sum_{i=1}^{n-1} 2\left(1 - \frac{i}{n}\right) r_i r_i'}$$

where n is the original number of data in each series and r_i and r_i' are the autocorrelations at lag i in the two data series, respectively.

2.1. Decadal Variability of Observed and Modeled GS Path and AMOC Fingerprint

The observed GS path and AMOC fingerprint show anticorrelated variations at time scales longer than 5 years (Figure 1a; $r = -0.81$ at zero lag, significant at 95% level). The observed AMOC fingerprint exhibits

Observed and Modeled Gulf Stream path and AMOC fingerprint
Observed GS path, AMOC fingerprint

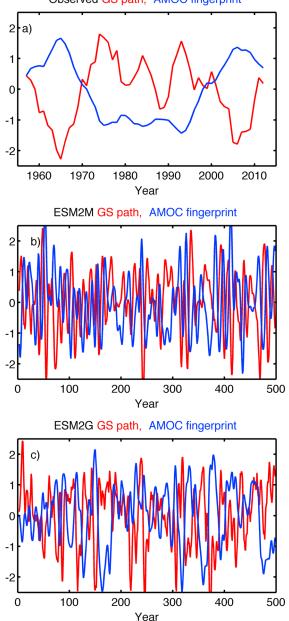ESM2M GS path, AMOC fingerprint

ESM2G GS path, AMOC fingerprint

Figure 1. Observed and simulated anomalies of the GS path (red) and AMOC fingerprint (blue). (a) Observed, (b) ESM2M, and (c) ESM2G. Both observed and modeled variables are filtered with a 5 year running mean and normalized by their standard deviations.

two strengthening periods, one from 1955 to 1965 and the other from 1993 to 2005. The strengthening of the AMOC is coincident with the southward shift of the GS path (Figure 1a). Similarly, for the two periods of AMOC weakening from 1965 to 1974 and from 2005 to present, the GS path shifted northward. The weakening of the AMOC since 2005 indicated by its fingerprint (Figure 1a) is consistent with the recent direct observational studies [*Robson et al.*, 2014; *Smeed et al.*, 2014] and the statistical prediction using the AMOC fingerprint [*Mahajan et al.*, 2011]. These findings are consistent with that found in *Joyce and Zhang* [2010] using unfiltered data, and here the anticorrelation between the 5 year smoothed observed GS path and AMOC fingerprint derived from the same objectively analyzed ocean temperature data sets [*Levitus et al.*, 2005] is much higher. Because the 5 year smooth reduces degrees of freedom for the limited observed time series, we also look into the squared coherence between the unsmoothed observed inverted GS path (where inverted means the sign of the GS path is reversed) and the AMOC fingerprint. There is significant high (at 95% level) squared coherence between the observed inverted GS path and AMOC fingerprint at decadal time scale and longer (Figure S2a).

Analogous to the observed results, the GS path and the AMOC fingerprint in the ESM2M and ESM2G control simulations show similar anticorrelated variability at decadal time scale (Figures 1b and 1c). The anticorrelation coefficient is $r = -0.80$ and -0.56 (significant at 99% level) in

ESM2M and ESM2G, when the enhanced (weakened) AMOC is leading southward (northward) GS path by ~2 and ~1 years, respectively. There is significant (at 95% level) squared coherence between simulated inverted GS path and AMOC fingerprint near decadal time scale in both ESMs (Figures S2c and S2e), similar to the observed (Figure S2a). In ESM2G, the peak of coherence is at a slightly higher frequency (~8 years). The ESMs simulate much lower coherence at multidecadal time scale than the observed (Figure S2); hence, the models are mainly used for understanding decadal variability. In ESM2M the variability of the AMOC/GS path is dominated by decadal time scale and is too small at multidecadal time scales (Figures 1b and 1c). In ESM2G, although the AMOC/GS path exhibits more variability at much longer (centennial) time scale (Figures 1b and 1c), the increase in the power spectra of AMOC/GS path variability from interannual to centennial time scale is much

greater than the increase in their squared cross-spectral density toward lower frequency (not shown), resulting in decreased squared-coherence from ~8 year to centennial time scales.

There is a difference in the frequency dependence of time lead between models and observations (Figures S2b, S2d, and S2f). At decadal time scale, unlike the in-phase relationship between the AMOC fingerprint and the inverted GS path in the observations (Figure S2b), the AMOC fingerprint leads the inverted GS path by ~2 years in ESM2M (Figure S2d) and by ~1 year in ESM2G (Figure S2f) due to the model bias. The GS region temperature anomaly in the simulated AMOC fingerprint in ESM2M is located too far east (near 50°W) compared with that in the observed AMOC fingerprint (near 75°W), and it takes ~2 years for this simulated temperature anomaly to propagate westward to 75°W. On the other hand, both modeled and observed GS path are dominated by temperature anomalies around 75°W; thus, the inverted GS path lags the AMOC fingerprint by ~2 years at decadal time scale in ESM2M (Figure S2d), while the inverted GS path is in phase with the AMOC fingerprint in the observations (Figure S2b). In ESM2G, the bias is not as far east as in ESM2M; hence, the inverted GS path only lags the AMOC fingerprint by ~1 year (Figure S2f). To verify the above model bias causing the difference in the time lead, we define an alternative GS path as the position of 200 m 15°C isotherm at 50°W in ESM2M and the position of 200 m 15°C isotherm averaged for 70°W–50°W in ESM2G, respectively, instead of the average of 75°W–55°W in the originals. Similar to that observed (Figures S2b and S3b), the inverted alternative GS path is almost in phase with the AMOC fingerprint in both ESMs, and there is not much frequency dependence (Figures S3d and S3f). The squared coherence at low frequency using the alternative GS path is also enhanced for both models (Figures S3c and S3e).

As discussed in previous studies [*Zhang*, 2008; *Zhang and Vallis*, 2007; *Zhang et al.*, 2011], a stronger (weaker) AMOC is associated with a stronger (weaker) North Atlantic deep flow, which interacts with the steep bottom topography near the North American east coast, and induces positive (negative) vorticity anomalies through bottom vortex stretching effects, resulting in a strengthening (weakening) of the cyclonic NRG and a southward (northward) shift of the GS path.
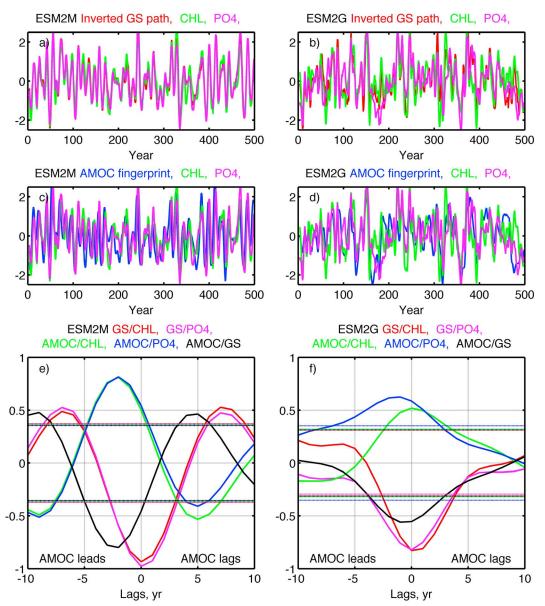
2.2. Decadal Variability of Chlorophyll and Nutrient Concentrations in the GS Region

This section analyzes the impact of AMOC variability on the chlorophyll and nutrient concentrations in the GS region. In ESM2M, both the chlorophyll index and the nutrient (PO_4) index are anticorrelated with the GS path at zero lag ($r = -0.93$, -0.97, respectively, significant at 99% level; Figures 2a and 2e). The AMOC fingerprint is positively correlated with both the chlorophyll index and the nutrient index with a 2 year lead ($r = 0.81$, 0.81, respectively, both significant at 99% levels) (Figures 2c and 2e). The leading mode of nutrient (PO_4) concentrations exhibits its highest anomalies along the GS path, especially in the region between 70°W and 55°W (Figure 3a). The leading mode of chlorophyll concentrations (Figure 4a) exhibits positive anomalies around the GS path as well as east of Georges Bank.

In ESM2G, the GS path is also anticorrelated with the chlorophyll index and the nutrient (PO_4) index at zero lag ($r = -0.83$, -0.82, respectively, both significant at 99% levels; Figures 2b and 2f). Meanwhile, the AMOC fingerprint is positively correlated with the chlorophyll index at zero lag ($r = 0.51$, significant at 99% level) and positively correlated with the nutrient (PO_4) index with a 1 year lead ($r = 0.62$, significant at 99% level) (Figures 2d and 2f). The leading mode of nutrient (PO_4) concentrations in ESM2G also shows positive anomalies along the GS path (Figure 3b) but has smaller amplitudes and extends further north than those in ESM2M (Figure 3a). In ESM2G the leading mode of chlorophyll concentrations exhibits strongest positive anomalies right north of the GS path (Figure 4b). Both ESMs results (Figure 2) suggest that the increases in chlorophyll and nutrient (PO_4) concentrations in the GS region occur when the GS path is shifted southward and the AMOC fingerprint is positive, and vice versa. The chlorophyll and nutrient variability in ESM2M is mainly at decadal time scale, whereas in ESM2G there is more biogeochemical variability at centennial time scale, consistent with the difference of AMOC variability in the two ESMs (Figure 2).

2.3. Mechanisms for Decadal Variability of Chlorophyll and Nutrient Concentrations

The climatological mean nutrient (PO_4) concentrations increase with latitude and depth in the GS region (Figures S4 and S5). For both ESMs, the anomalous nutrient (PO_4) concentrations regressed on the inverted GS path (Figures 3c and 3d) show very similar spatial patterns as the corresponding leading modes in PO_4 concentrations (Figures 3a and 3b), indicating the variability of the GS path dominates the anticorrelated variability of nutrient concentrations in the GS region. The region north of the GS path typically features high
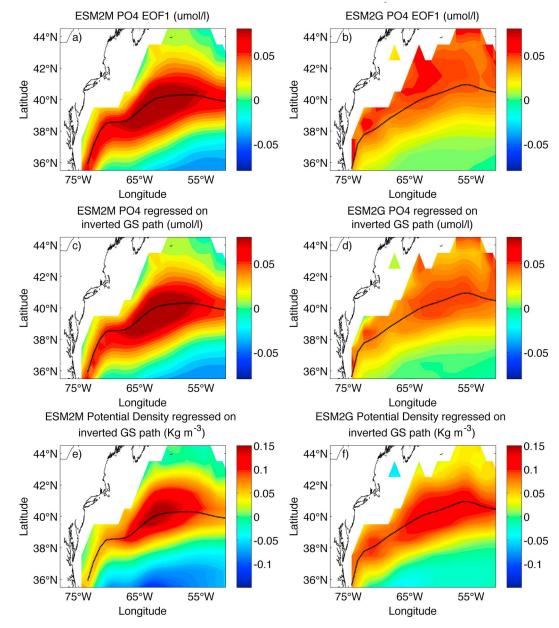
Figure 2. Simulated physical and biogeochemical variables from two ESMs (Left—ESM2M, and right—ESM2G). (a–d) Inverted GS path (red), AMOC fingerprint (blue), chlorophyll index (green), and PO$_4$ index (purple). A 5 year running mean is applied and all variables are normalized by their standard deviations. (e and f) Cross correlations among the variables shown in Figures 2a–2d the dashed lines are 99% significance levels for each pair of variables with the two-tailed Student's t test.

climatological chlorophyll concentrations associated with the spring bloom (Figure S6). For both ESMs, the anomalous chlorophyll concentrations regressed on the inverted GS path (Figures 4c and 4d) exhibit very similar spatial patterns to the corresponding leading modes in chlorophyll concentrations (Figures 4a and 4b), indicating that the variability of chlorophyll concentration in this region is strongly linked to the anti-correlated variability in the GS path. Next, mechanisms for the above linkages are explained; i.e., nutrient reservoirs vary with isopycnal changes in the GS front induced by the AMOC variability, resulting in variations in chlorophyll concentrations in this region.
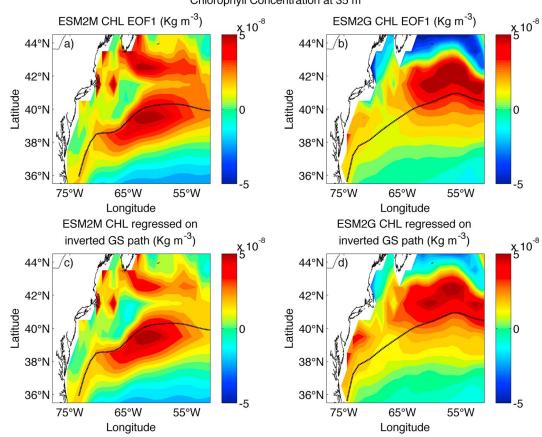
Figures 3e and 3f show the anomalous annual mean potential density at 150 m regressed on the inverted GS path in ESM2M and ESM2G, respectively. The GS path-centric pattern is strikingly similar to the spatial distribution in the corresponding leading modes in nutrient concentrations in both ESMs, although it is more
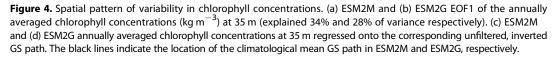
PO4 Concentration and Potential Density at 150 m

Figure 3. Spatial pattern of variability in PO_4 concentrations and potential density. (a) ESM2M and (b) ESM2G EOF1 of the annually averaged PO_4 concentrations (μmol/l) at 150 m (explained 52% and 47% of variance respectively). (c) ESM2M and (d) ESM2G annually averaged PO_4 concentrations at 150 m regressed onto the corresponding unfiltered, inverted GS path. (e) ESM2M and (f) ESM2G annually averaged potential density (kg m^{-3}) at 150 m regressed onto the corresponding unfiltered, inverted GS path. The black lines indicate the location of the climatological mean GS path in ESM2M and ESM2G, respectively.

apparent for ESM2M than for ESM2G. This implies that the GS path-centric pattern in the variability of nutrient concentrations is closely tied to changes in isopycnals. In both ESMs, there are strong correlations between anomalous nutrient concentrations and potential density in the region of the mean GS path, indicating a robust direct relationship between them (Figure S7). The positive potential density anomalies at this depth (i.e., shallowing of isopycnals) are associated with southward shifts in the GS path, and vice versa. A stronger AMOC leads to steepened isopycnal slopes in the GS front (mainly due to the strengthening of the cyclonic NRG cooling the region north of the GS path), as well as a southward shift of the GS front. Hence, the isopycnals are shallower and nutrient concentrations are higher along the climatological mean GS path as well as

Figure 4. Spatial pattern of variability in chlorophyll concentrations. (a) ESM2M and (b) ESM2G EOF1 of the annually averaged chlorophyll concentrations (kg m^{-3}) at 35 m (explained 34% and 28% of variance respectively). (c) ESM2M and (d) ESM2G annually averaged chlorophyll concentrations at 35 m regressed onto the corresponding unfiltered, inverted GS path. The black lines indicate the location of the climatological mean GS path in ESM2M and ESM2G, respectively.

north of it, and the isopycnals are deeper and nutrient concentrations are lower in the south. Note that the amplitude of the anomalous potential density near the GS path is smaller in ESM2G than in ESM2M (Figures 3e and 3f); consequently, the amplitude of the anomalous nutrient concentrations near the GS path is also smaller in ESM2G than in ESM2M (Figures 3c and 3d).

Levy et al. [2009] found that the subsurface nutrient concentrations in the western North Atlantic change with the isopycnals; i.e., higher nutrient concentrations (shallowing of nutriclines) are associated with shallowing isopycnals in the region north of the subtropical gyre, and lower nutrient concentrations (deepening of nutriclines) are associated with the deepening of isopycnals in the subtropical gyre as a result of the gyre boundary shifting south. Here we specifically found that the variability of the subsurface nutrient distribution in the GS region is linked to the variability of the AMOC/GS path through isopycnal changes in the GS front.

The enhanced nutrient in the GS region has contributed to the enhanced chlorophyll concentrations around the GS path. However, the spatial patterns of anomalous chlorophyll concentrations do not match the spatial patterns for anomalous nutrient concentration exactly (Figures 3c and 3d and Figures 4c and 4d); i.e., the maximum anomalies in chlorophyll concentrations are located slightly south in ESM2M and slightly north in ESM2G than the locations for the maximum anomalies in nutrient concentration. This is because the response of chlorophyll concentrations to changes in nutrient concentrations is nonlinear and depends on the climatological mean nutrient concentrations [*Follows and Dutkiewicz*, 2002]. In regions with relatively high climatological mean nutrient concentrations, chlorophyll concentrations are less sensitive to the increase in nutrient concentrations, and other factors such as light limitation dominate the response. In regions with relatively low climatological mean nutrient concentrations, chlorophyll concentrations are more likely to be affected by nutrients and are thus more sensitive to the increase in nutrient concentrations. In ESM2M, the region with

relatively low climatological mean nutrient concentrations at 150 m shifts southward compared with that in the observed (Figure S4); hence, the region with the maximum anomalies in chlorophyll concentrations shifts southward to slightly south of the GS path (Figure 4c). In ESM2G, the region with relative low climatological mean nutrient concentrations at 150 m shifts northward compared with that in the observed (Figure S4); hence, the region with the maximum anomalies in chlorophyll concentrations also shifts northward to slightly north of the GS path (Figure 4d). In addition, the positive anomalies in chlorophyll concentrations east of Georges Bank in ESM2M (Figure 4c) are mainly induced by the stronger upwelling north of the GS path, as diagnosed from stronger vertical mass transport in this region associated with the southward shift of the GS path (not shown). An increase in upwelling would lead to increased nutrient supply, consequently increasing the chlorophyll concentrations for this region. The vertical mass transport/vertical velocity variables are not available from ESM2G outputs, so changes in the upwelling could not be revealed by ESM2G.

Schollaert et al. [2004] and *Saba et al.* [2015] found that at interannual time scale, a northward shift in the GS position coincides with an increase in the spring bloom over the U.S. shelf/Slope Sea region using satellite data. Here our modeling results are focused on chlorophyll concentrations further south (away from the U.S. shelf break) around the GS path, and satellite data indeed show anticorrelations between the GS path and spring chlorophyll concentrations around the GS path at interannual time scale (Vincent Saba, personal communication), consistent with our modeling results. The currently available observed data for chlorophyll/nutrient concentrations in the GS region are still too short to verify the decadal variability discussed here.

3. Conclusions and Discussions

To summarize, results here suggest that the underlying physical driver for the decadal variability in the GS path and the regional biogeochemical cycle is linked to the low frequency variability in the AMOC. An enhanced AMOC leads to a stronger cyclonic NRG thus cooling in the Slope Sea, as well as a southward shift of the GS path, results in steepened isopycnal slopes in the GS front. Nutrient reservoirs in the GS region move along with the steepened isopycnals in the GS front induced by the enhanced AMOC; hence, nutrient concentrations are higher along the GS path in response to the shallower isopycnals there. The enhanced nutrient concentrations in the GS region have contributed to the enhanced chlorophyll concentrations around the GS path. These results suggest that physical processes are a significant driving mechanism for the simulated decadal biogeochemical variability in the GS region. The impact of the AMOC and the GS path on the decadal variability of another nutrient, nitrate (NO_3), is very similar to that found for phosphate (PO_4). The analysis of the full biogeochemical cycle in the GS region is beyond the scope of this paper.

Our results have shown how changes in basin wide ocean circulation, such as AMOC, are teleconnected with regional scale physical and biogeochemical variations near the U.S. eastern seaboard at decadal time scales; such connections are useful for understanding and predicting future physical and biogeochemical variations near the North American east coast. Further, AMOC-induced decadal variability in chlorophyll and nutrient concentrations in the GS region might be important for changes in the localized carbon cycle and fisheries at decadal time scale.

Last, we note that differences in the simulated chlorophyll and nutrient concentrations in the GS region between ESM2M and ESM2G might be attributed to differences in the oceanic physical components between the two ESMs. Nevertheless, the simulated impact of the AMOC and the anticorrelated GS path on the decadal variability in chlorophyll and nutrient concentrations in the GS region are generally consistent between the two ESMs, suggesting the robustness of the results. However, caution is advised when linking the GS variability and biogeochemical cycling in coarse resolution models with biased mean states [*Henson et al.*, 2009]. The ESMs results here need to be compared with high resolution ESMs in the future.

References

Behrenfeld, M., R. O'Malley, D. Siegel, C. McClain, J. Sarmiento, G. Feldman, A. Milligan, P. Falkowski, R. Letelier, and E. Boss (2006), Climate-driven trends in contemporary ocean productivity, *Nature*, 444, 752–755.
Cornillon, P., and R. D. Watts (1987), Satellite thermal infrared and inverted echo sounder determinations of the Gulf Stream Northern Edge, *J. Atmos. Oceanic Technol.*, 4, 712–723.
Csanady, G. T. (1990), Physical basis of coastal productivity, *Eos Trans. AGU*, 71, 1060–1065.
Cunningham, S. A., et al. (2007), Temporal Variability of the Atlantic Meridional Overturning Circulation at 26.5°N, *Science*, 317, 935–938.

De Coetlogon, G., C. Frankignoul, M. Bentsen, C. Delon, H. Haak, S. Masina, and A. Pardaens (2006), Gulf Stream variability in five oceanic General circulation models, *J. Phys. Oceanogr.*, *36*, 2119–2135.

Doney, S. C. (2006), Plankton in a warmer world, *Nature*, *444*, 695–696.

Dunne, J. P., et al. (2012), GFDL's ESM2 Global Coupled Climate-Carbon Earth System Models. Part I: Physical formulation and baseline simulation characteristics, *J. Clim.*, *25*, 6646–6665.

Dunne, J. P., et al. (2013), GFDL's ESM2 Global Coupled Climate-Carbon Earth System Models. Part II: Carbon system formulation and baseline simulation characteristics, *J. Clim.*, *26*, 2247–2267.

Follows, M., and S. Dutkiewicz (2002), Meteorological modulation of the North Atlantic spring bloom, *Deep Sea Res., Part II*, *49*, 321–344.

Frankignoul, C., G. De Coetlogon, T. Joyce, and S. Dong (2001), Gulf Stream variability and ocean–atmosphere interactions, *J. Phys. Oceanogr.*, *31*, 3516–3528.

Fuglister, F. C., and A. D. Voorhis (1965), A new method of tracking the Gulf Stream, *Limnol. Oceanogr.*, *10*, 115.

Henson, S. A., D. Raitsos, J. P. Dunne, and A. McQuatters-Gollop (2009), Decadal variability in biogeochemical models: Comparison with a 50-year ocean colour dataset, *Geophys. Res. Lett.*, *36*, L21601, doi:10.1029/2009GL040874.

Jenkins, W. J., and S. C. Doney (2003), The subtropical nutrient spiral, *Global Biogeochem. Cycles*, *17*(4), 1110, doi:10.1029/2003GB002085.

Joyce, T., and R. Zhang (2010), On the path of the Gulf Stream and the Atlantic meridional overturning circulation, *J. Clim.*, *23*(11), 3146–3154.

Joyce, T., C. Deser, and M. A. Spall (2000), The relation between decadal variability of subtropical mode water and the North Atlantic Oscillation, *J. Clim.*, *13*, 2550–2569.

Joyce, T., Y.-O. Kwon, and L. Yu (2009), On the relationship between synoptic wintertime atmospheric variability and path shifts in the Gulf Stream and Kuroshio Extension, *J. Clim.*, *22*, 3177–3192.

Kremeur, A.-S., M. Levy, O. Aumont, and G. Reverdin (2009), Impact of the subtropical mode water biogeochemical properties on primary production in the North Atlantic: New insights from an idealized model study, *J. Geophys. Res.*, *114*, C07019, doi:10.1029/2008JC005161.

Kwon, Y.-O., M. A. Alexander, N. A. Bond, C. Frankignoul, H. Nakamura, B. Qiu, and L. Thompson (2010), Role of Gulf Stream and Kuroshio-Oyashio Systems in large-scale atmosphere–ocean interaction: A review, *J. Clim.*, *23*, 3249–3281.

Levitus, S., J. Antonov, and T. Boyer (2005), Warming of the world ocean, 1955–2003, *Geophys. Res. Lett.*, *32*, L02604, doi:10.1029/2004GL021592.

Levy, M., D. Iovino, S. Masson, G. Madec, P. Klein, A.-M. Treguier, and K. Takahashi (2009), Remote impacts of Sub-Mesoscale Dynamics on new production, *Mercator Ocean Quart. Newslett.*, *35*, 13–19.

Lozier, M. S., A. C. Dave, J. B. Palter, L. M. Gerber, and R. T. Barber (2011), On the relationship between stratification and primary productivity in the North Atlantic, *Geophys. Res. Lett.*, *38*, L18609, doi:10.1029/2011GL049414.

Mahajan, S., R. Zhang, T. Delworth, S. Zhang, A. Rosati, and Y.-S. Chang (2011), Predicting Atlantic meridional overturning circulation (AMOC) variations using subsurface and surface fingerprints, *Deep Sea Res., Part II*, *58*, 1895–1903.

Marshall, J., H. Johnson, and J. Goodman (2001), A Study of the interaction of the North Atlantic Oscillation with Ocean Circulation, *J. Clim.*, *14*, 1399–1421.

Martinez, E., D. Antoine, F. D'Ortenzio, and B. Gentili (2009), Climate-driven basin-scale decadal oscillations of oceanic phytoplankton, *Science*, *326*, 1253–1256.

Minobe, S., A. Kuwano-Yoshida, N. Komori, S.-P. Xie, and R. J. Small (2008), Influence of the Gulf Stream on the trophosphere, *Nature*, *452*, 206–209.

Nye, J., T. Joyce, Y.-O. Kwon, and J. S. Link (2011), Silver hake tracks changes in Northwest Atlantic circulation, *Nat. Commun.*, *2*, 412, doi:10.1038/ncomms1420.

Palter, J. B., and M. S. Lozier (2008), On the source of Gulf Stream nutrients, *J. Geophys. Res.*, *113*, C06018, doi:10.1029/2007JC004611.

Pelegri, J. L., and G. T. Csanady (1991), Nutrient transport and mixing in the Gulf Stream, *J. Geophys. Res.*, *96*, 2577–2583.

Robson, J., D. Hodson, E. Hawkins, and R. Sutton (2014), Atlantic overturning in decline?, *Nat. Geosci.*, doi:10.1038/ngeo2050.

Saba, V. S., K. J. W. Hyde, N. D. Rebuck, K. D. Friedland, J. A. Hare, M. Kahru, and M. J. Fogarty (2015), Physical associations to spring phytoplankton biomass interannual variability in the U.S. Northeast Continental Shelf, *J. Geophys. Res. Biogeosci.*, *120*, 205–220, doi:10.1002/2014JG002770.

Schollaert, S. E., H. T. Rossby, and J. A. Yoder (2004), Gulf Stream cross-frontal exchange: Possible mechanisms to explain interannual variations in phytoplankton chlorophyll in the Slope Sea during SeaWiFS years, *Deep Sea Res., Part II*, *51*, 173–188.

Smeed, D. A., et al. (2014), Observed decline of the Atlantic meridional overturning circulation 2004–2012, *Ocean Sci.*, *10*, 29–38.

Spall, M. A. (1996), Dynamics of the Gulf Stream/Deep Western Boundary Current Crossover. Part I: Entrainment and Recirculation, *J. Phys. Oceanogr.*, *26*, 2152–2168.

Taylor, A. H., and J. A. Stephens (1998), The North Atlantic Oscillation and the latitude of the Gulf Stream, *Tellus A*, *50*, 134–142.

Thompson, D. J., and W. J. Schmitz (1989), A Limited-Area Model of the Gulf Stream: Design, Initial Experiments, and Model-Data Intercomparison, *J. Phys. Oceanogr.*, *19*, 791–814.

Williams, R. G., V. Roussenov, and M. J. Follows (2006), Nutrient streams and their induction into the mixed layer, *Global Biogeochem. Cycles*, *20*, GB1016, doi:10.1029/2005GB002586.

Yeager, S., and M. Jochum (2009), The connection between Labrador Sea buoyancy loss, deep western boundary current strength, and Gulf Stream path in an ocean circulation model, *Ocean Modell.*, *30*, 207–224.

Zhang, R. (2008), Coherent surface-subsurface fingerprint of the Atlantic meridional overturning circulation, *Geophys. Res. Lett.*, *35*, L20705, doi:10.1029/2008GL035463.

Zhang, R., and G. Vallis (2007), The Role of Bottom Vortex Stretching on the Path of the North Atlantic Western Boundary Current and on the Northern Recirculation Gyre, *J. Phys. Oceanogr.*, *37*(8), 2053–2080.

Zhang, R., T. Delworth, A. Rosati, W. Anderson, K. Dixon, H.-C. Lee, and F. Zeng (2011), Sensitivity of the North Atlantic Ocean circulation to an abrupt change in the Nordic Sea overflow in a high resolution global coupled climate model, *J. Geophys. Res.*, *116*, C12024, doi:10.1029/2011JC007240.